Lawrence Berkeley Laboratory

UNIVERSITY OF CALIFORNIA
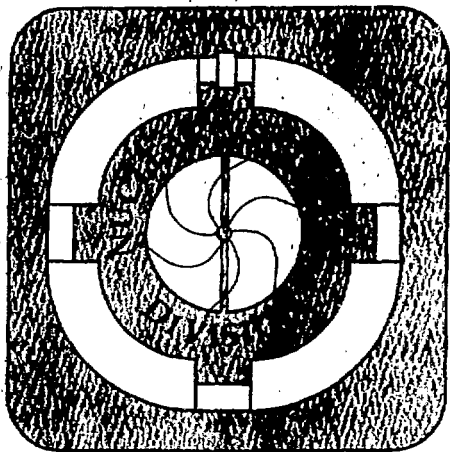
ECR ION SOURCES FOR CYCLOTRONS

C.M. Lyneis

October 1986

ECR ION SOURCES FOR CYCLOTRONS*

C. M. LYNEIS

Nuclear Science Division, Lawrence Berkeley Laboratory,
University of California, Berkeley, California 94720, USA

MASTER

ECR ION SOURCES FOR CYCLOTRONS*

C. M. LYNEIS

Nuclear Science Division, Lawrence Berkeley Laboratory,
University of California, Berkeley, California 94720, USA

Introduction

In the last decade ECR (Electron Cyclotron Resonance) ion sources have evolved from a single large, power consuming, complex prototype into a variety of compact, simple, reliable, efficient, high performance sources of high charge state ions for accelerators and atomic physics. The coupling of ECR sources to cyclotrons has resulted in significant performance gains in energy, intensity, reliability, and variety of ion species. Seven ECR sources are in regular operation with cyclotrons and numerous other projects are under development or in the planning stage. At least four laboratories have ECR sources dedicated for atomic physics research and other atomic physics programs share ECR sources with cyclotrons. An ECR source is now installed on the injector for the CERN SPS synchrotron to accelerate O^{8+} to relativistic energies. A project is underway at Argonne to couple an ECR source to a superconducting heavy-ion linac. Although tremendous progress has been made, the field of ECR sources is still a relatively young technology and there is still the potential for further advances both in source development and understanding of the plasma physics.

Five main topics will be covered in this paper. First the development of ECR sources will be reviewed. Second, the important physics mechanisms which come into play in the operation of ECR Sources will be discussed, along with a discussion of various models for charge state distributions (CSD). Third, the design and performance of several ECR sources will be compared. Fourth, we will use the 88-Inch Cyclotron and the LBL ECR as an example of cyclotron+ECR operation. Finally, we will look to the future of ECR sources.

Development of ECR Sources.

The field of ECR ion sources has its roots in the plasma fusion developments in the late 1960's and early 1970's. The use of ECRH (Electron Cyclotron Resonance Heating) in plasma devices to produce high charge state ions was suggested in 1969 [1], and the first extracted beams from these devices were reported in 1972.[2,3] Although these devices, which used solenoid

magnetic mirror configuration were capable of producing plasma densities on the order of 1×10^{12} cm^{-3} and keV electrons, typical operating pressures were 10^{-4} to 10^{-5} Torr and the ion confinement times were 10^{-4} s or less. This resulted in CSD for nitrogen peaked on N^{2+} and for argon peaked at Ar^{2+}.

In 1973 Geller converted a large mirror device (CIRCE) used in plasma fusion research into an ion source (SUPERMAFIOS).[4] Unlike the earlier ion sources using ECRH, the magnetic field of SUPERMAFIOS used a hexapolar field in addition to the usual solenoidal mirror field. This produced a minimum B magnetic field configuration which stabilized the plasma against MHD instability. This effect was first demonstrated in a plasma fusion device in 1961.[5] Several configurations of the ECR source SUPERMAFIOS A, Triple-MAFIOS, and finally SUPERMAFIOS B were tested between 1974 and 1977. The second major innovation during the development of SUPERMAFIOS was the addition of a first stage which operated at higher pressure and produced a dense cold plasma which flowed into the second stage.[6] As discussed later, both the minimum B configuration and two stages appear to be crucial for optimum high charge state performance. Except for the large size (length 100 cm and diameter 35 cm) and large power consumption of the normal conducting solenoids and hexapolar coils (3 MW), the SUPERMAFIOS B machine had all the essential characteristics of all recent ECR ion sources. In SUPERMAFIOS B the $n_e \tau_i$ was $\sim 3 \times 10^9$ cm^{-3}s, which is sufficient to produce some fully stripped light ions. The INTEREM device at Oak Ridge was another plasma fusion device converted into an ion source. It used a combination of solenoid and quadrupole coils to produce a minimum B geometry. Although this device succeeded in producing a nitrogen CSD peaked on N^{3+} with a small amount of N^{6+}, the extraction geometry was very inefficient and the resulting currents were too small for practical use.[7]

The success of SUPERMAFIOS resulted in new efforts to develop a practical ECR source for use with cyclotrons and in atomic physics. In Louvain-la-Neuve a project to build a large superconducting ECR similar in size and configuration to SUPERMAFIOS was undertaken.[8] In the meantime, MICROMAFIOS a small ECR source utilizing SmCo$_5$ permanent magnets to produce the hexapolar field was developed and tested.[9] In Karlsruhe a large source utilizing superconducting solenoids and a SmCo$_5$ hexapole was built.[10] As shown in Table 1, since these pioneering efforts, the number and variety of ECR sources has grown rapidly. MINIMAFIOS sources built in Grenoble by Geller's group are in regular operation with cyclotrons at KVI in Gronnigen, SARA Grenoble, and GANIL in Caen.

The performance of the ECR ion sources has increased steadily and there are a number of ECR sources built in different laboratories, that are producing excellent results. At the most recent ECR Ion Source Workshop, similar performance was reported with gases such as oxygen and argon for the following sources: MINIMAFIOS-10GHz, the ORNL-ECR, the LBL-ECR, OCTOPUS, the MSU-ECR, ISIS, and ECREVIS. The plasma chambers of these sources range in size from a length of 30 cm and a diameter of 7 cm in MINIMAFIOS to a length of 120 cm and a diameter of 32 cm in ECREVIS and the second stage RF frequencies range from 6.4 GHz for the LBL-ECR to 14.3 GHz for ISIS. The similarity in the CSD and

TABLE 1
ECR ION SOURCES

SOURCE	LAB	1st Op.	L (cm)	D (cm)	F (GHz)	COMMENTS	APPL
SUPERMAFIOS	Grenoble	1974	100	35	16,8	3 MW used.	Test
MICROMAFIOS	Grenoble	1979	30	7	10	Compact, copper coils,SmCo	Test
MINIMAFIOS	Grenoble	1980	30	7	10	Now at KVI, SARA,GANIL	Test, A.P. &Cyc.
p-HISKA	Karlsruhe	1980	28	7	14.5,7.5	Compact,SmCo	Test&Cyc
GSI-ECR	Darmstadt	1980	15	2.5	14.3	Single stage, Iron yoke	Test
ECREVETTE	L-L-N	1981	40	12	14.7,8.5	1st s.c. ECR	Test&Cyc
HISKA	Karlsruhe	1982	70	10	14, 7.5	s.c. Solenoids, SmCo Sextupole	Cyc
Pre-ISIS I	Jülich	1981	25	5	2.5	Small, low freq. Single stage	Test
Pre-ISIS II	Jülich	1982	25	5	5	Two stage	Test&Cyc
ECREVIS	L-L-N	1982	120	32	14.7, 8.5	Large s.c. ECR	Cyc, A.P.
LISKA	Karlsruhe	1984	25	7	7.5	Lithium ECR	Cyc
ONRL-ECR	Oak Ridge	1984	40	8.5	10.6	Compact,SmCo	At.Phys.
LBL-ECR	Berkeley	1984	33	9.	9.2, 6.4	Open sextupole	Cyc.,A.P
MINIMAFIOS-16GHz	Grenoble	1984	30	7	16.6	Pulsed source	Test
CAPRICE	Grenoble	1984	13.5	8	10	Iron yoke, very compact	Test
ECR2	RIKEN	1985	30	8	2.5,2.5	Whistler mode heating	Test
MSU-ECR	E. Lansing	1985	50	14	6.4,6.4	Iron yoke, 1st stage sextupole	Cyc
OCTOPUS	L-L-N	1985	70	18	14.3,8.5	Iron yoke, open octupole	Cyc, A.P.
ISIS	Jülich	1985	70	20	14.3,14.3	Large s.c, high freq	Cyc
MINIMAFIOS-18 GHz	Grenoble	1986	30	7	18	Highest Freq ECR	Test,Sync

extracted ion intensities of these sources seems to indicate that they are are all operating with similar $n_e \tau_i$ products.

Physics of ECR Ion Sources

Although the basic concepts involved in ECR ion sources are straight forward, developing an accurate model to predict their performance requires detailed understanding of a variety of atomic physics and plasma physics processes. The atomic physics processes include electron impact ionization, ion-ion charge exchange, ion-neutral charge exchange, electron-electron scattering, electron capture by ions, and electron-ion scattering. The plasma physics processes include magnetic confinement, stochastic heating of electrons by ECRH, plasma potentials, microinstabilities, and wave propagation in plasmas.

The basic figure of merit for an ECR ion source plasma is $n_e \tau_i$ where n_e is the plasma density and τ_i is the ion confinement time. The equilibrium CSD in an ECR ion source is determined by the balance between the ion production rate (proportional to n_e) with the ion loss rate (proportional to τ_i). The high charge state ions are generated by sequential ionization from electron impact. The rate at which ions of charge i are produced by electron impact ionization is given by

$$R_{prod,i} = n_e \langle \sigma_{i-1,i} v_e \rangle n_{i-1} \qquad \text{Eq(1)}$$

where n_e is the electron density, $\langle \sigma_{i-1,i} v_e \rangle$, the rate coefficient is the product of the electron impact ionization cross section from charge state i-1 to i times v_e the electron velocity averaged over the electron energy distribution, and n_{i-1} the density of ions of charge state i-1. The loss rate for ions charge state i is given by

$$R_{loss,i} = n_o \langle \sigma_{o,i} v_i \rangle n_i + n_i \tau_i^{-1} \qquad \text{Eq(2)}$$

where n_o is the density of neutral atoms in the plasma, $\sigma_{o,i}$ is the ion neutral charge exchange cross section, v_i is the ion velocity. The brackets indicate an average over the ion energy distribution function. Combining the ionization and loss rates gives the rate of change for ion charge state i

$$\frac{dn_i}{dt} = n_e \langle \sigma_{i-1,i} v_e \rangle n_{i-1} + n_o \langle \sigma_{o,i+1} v_{i+1} \rangle n_{i+1}$$

$$- n_e \langle \sigma_{i,i+1} v_e \rangle n_i - n_o \langle \sigma_{o,i} v_i \rangle n_i - \frac{n_i}{\tau_i} \qquad \text{Eq(3)}$$

In equilibrium the rate of change is zero and Eq(3) gives a set of coupled equations for i=1 to z_{max} which can be solved for the CSD assuming the plasma density, electron temperature, ion

temperature, neutral density, ion confinement time, and the appropriate cross sections are known.

Solutions to these equations have been developed by a number of authors.[11-15] BALANC developed by Jongen[14] is one of the computer codes which simulates the CSD and has been used by the author to fit the CSD of the LBL ECR. This code evolved from a preliminary attempt by Chan-Tung[13], was developed by Jongen, improved by West[15], and then further modified by Jongen. A rather complete description of the physics and the formulas used in the code is given by West.[15]   The weak point of all of these models is in the calculation of τ_i.   In BALANC the ion confinement times are computed using a model incorporating diffusion along the source axis and an electrostatic potential which gives

$$\tau_i \propto \frac{L^2 \sqrt{m}\ z_i^2\ z_{eff}^2\ n_i}{T_i^{5/2}\ \left(1 + \dfrac{z_i V}{T_i}\right)} \qquad\qquad Eq(4)$$

where L is the plasma chamber length, m the ion mass, z_i the charge state, z_{eff} an effective mean charge in the plasma, $n_{i,eff}$ an effective ion density, T_i the ion kinetic energy, and V the plasma potential. V is function of the source geometry and plasma parameters. Although this model clearly has some flaws it is interesting to note that it predicts that the ion confinement time increases a z_i^2 and $\sqrt{m}$. Geller suggested earlier that the ion confinement time was determined by ion-ion scattering along the axis which gives an expression similar to Eq(4) without the term in brackets.[4] In West's code (ECRCSD) the confinement time was based on a plasma potential trap model developed for the plasma fusion mirror devices. This predicts a slower increase in τ_i with increasing charge state than Eq(4). Wiesemann's approach is to treat τ_i as a fit parameter independent of charge state.[16] Unfortunately, none of these approaches is free from questionable assumptions, but it may be possible to test the dependence of τ_i on ion charge state by comparing the CSDs calculated using each model to experimental charge state distributions. Measurements on the LBL ECR using a mixture of ^{16}O and ^{18}O showed the CSD for ^{18}O was enhanced relative to ^{16}O. This enhancement was approximately consistent with an τ_i increasing as $\sqrt{m}$. Since this measurement was made for both isotopes in the same plasma, it clearly points to a mass dependence for τ_i.

Now we will examine how well the various cross sections, velocities, and densities can be calculated or inferred from measurements. Considerable experimental data on electron impact ionization cross sections already exists and the use of ECR sources by atomic physics groups will extend these measurements to higher charge state ions. Crandal reviewed the cross section data and models in 1981 and found that the semi-empirical Lotz formula was the best general model.[17,18] For low Z atoms single step ionization is the dominant mechanism, whereas for high Z atoms such as xenon multi-step ionization becomes important as Müller pointed out

recently. [19] He showed that assuming Lotz cross sections for xenon can result in significant errors in the CSD for an EBIS and this is also true for ECR source calculations. In Fig. 1, two calculated CSD using different electron impact ionization cross sections are compared to a measured CSD for oxygen from the LBL ECR. The Lotz cross section give a much better fit than the Müller-Salszborn cross sections. This is not surprising since the Müller-Salzborn formula was developed specifically to model argon and should not be expected to give accurate cross sections for other elements.[20,21] In Fig 2 ionization cross sections for argon calculated using MS are illustrated.[22] Experimental CSD for argon from the LBL ECR are better fit using MS than Lotz cross sections. Figure 1 illustrates that the detailed shape of the CSD depends strongly on the electron impact ionization cross sections.

Another uncertainty in determining the electron impact ionization cross sections concerns the electron energy distribution in the plasma. Three electron distribution functions have been used in modeling the CSD from ECR sources. They are a Maxwellian distribution,[14] a two component distribution with cold electrons and a Maxwellian hot electron distribution,[15] and a power law distribution function.[16] In principle, the electron distribution function can be determined by measuring the x-ray bremsstrahlung spectrum from the plasma. These measurements are made difficult by the high energy x-rays produced by hot electron collisions with the chamber walls and by experimental difficulties involved in measuring x-rays below 2 keV. Bernhardi et al[23] found a power law dependence for the electron distribution function measured on their simple mirror ECR source. They used careful shielding so that the Ge detector saw only the bremsstrahlung from the plasma for energies above 2 keV and used a retarding field analyzer for lower energy electrons. It is not clear that this data from this simple mirror device which operated at pressures a factor of 10 higher than a typical ECR source applies to one with a minimum B geometry. At M.I.T. extensive electron distribution measurements have been made on Constance-B, which is a plasma fusion device used to explore ECRH.[24] It is a minimum B structure using a baseball coil structure to produce a radial quadrupole field and an axial mirror field. They used an intrinsic planar Ge soft x-ray detector to measure the bremsstrahlung x-ray spectrum between 2 keV and 150 keV. The measurements indicated that the the spectrum was Maxwellian down to 2 keV. Although the Constance B operating parameters are similar to that of an ECR source, the differences in geometry and lack of a first stage make these results difficult to apply. In any case, without such elaborate measurement being made in coincidence with the measurements of the CSD the electron temperature must be treated as a free parameter in modeling.

The plasma density can be determined by RF transmission measurements across the plasma or by measuring the plasma diamagnetism. An upper limit to the plasma density, at least in the second stages of existing ECR sources is given by the plasma critical density

$$n_{ec} = 1.24 \times 10^{-8} f^2 \qquad \text{Eq(5)}$$

where f is the microwave frequency. For example, at 10 GHz the critical density is 1.24×10^{12}

OXYGEN CSD CALCULATED AND MEASURED
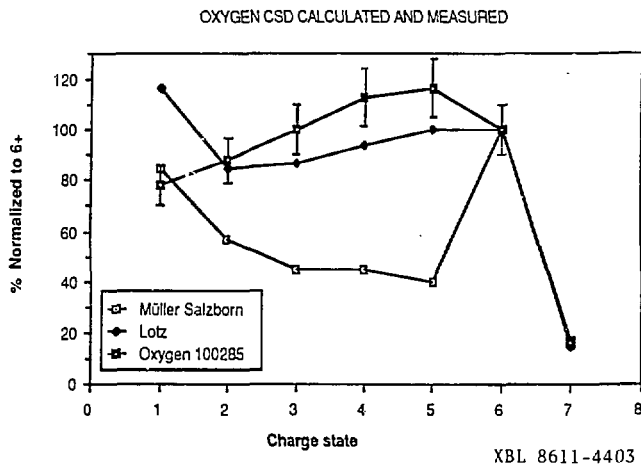

XBL 8611-4403

Fig. 1. Comparison of the measured charge state distribution (CSD) of oxygen from the LBL ECR with calculated CSD using Jongen's code with Lotz cross sections and Müller Salzborn cross sections. Parameters for Lotz are $p = 8 \times 10^{-7}$ Torr, $n_e = 3 \times 10^{11}$ cm^{-3}, $E_e = 2000$ eV, $T_i = 5$ eV, $T_o = 3000$ °K, and $V_p = 0$ V. Parameters for Muller Salzborn are the same except $E_e = 1000$ ev.
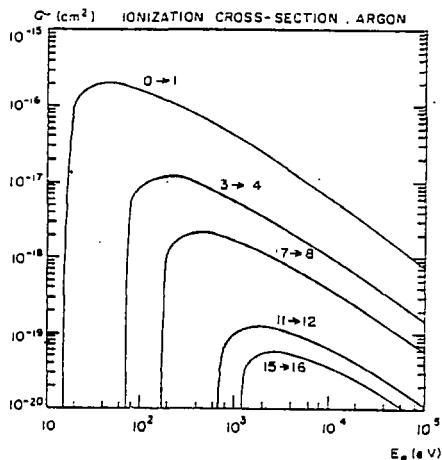

Fig. 2 Computer calculation of some argon electron impact ionization cross sections using Müller Salzborn formula.[22]

XBL 8611-4404

cm^{-3}. Although there are numerous examples of overdense plasmas in the literature attempts to use them in ECR sources have not yet been successful. Relatively little has been published about experimental determinations of the second stage plasma density of ECR sources. The density in TRIPLEMAFIOS was measured to be $\sim 2 \times 10^{11} cm^{-3}$. [4] The plasma diamagnetism is proportional to the $n_e T_e$ where T_e is the kinetic energy of the electrons in the plasma. The diamagnetism must be measured outside the ECR zone to avoid destruction of the measuring loop or probe and therefore the resulting density inferred depends on the assumptions made about the radial distribution of the plasma. Measurements on OCTOPUS using a Hall probe were consistent with a density of $3 \times 10^{+11}$ cm^{-3} at an energy of 4 keV. [25] Extensive measurements have been made on the Constance B plasma device,[22] where they found a hot electron density of 1×10^{11} cm^{-3} and a cold electron density of 2×10^{11} cm^{-3}. The measured hot electron density in INTEREM was 3×10^{11} cm^{-3}. [7]

In contrast to the uncertainty in the electron temperatures, two groups have measured the ion energies recently. Meyer found that the ion temperatures in the ORNL ECR were $T_i/q_i \le 5$ eV where q_i is the ion charge state.[26] H. Köhler et al [27] found the ion energy distribution of the extracted beam to be consistent with an accelerated Maxwellian distribution again with T_i/q_i on the order a a few eV depending somewhat on what gas was used.

Design and Performance of ECR sources

Although the structure of this paper with a theoretical discussion prior to the practical section might seem to imply that the theory is more important to the development of ECR sources than experiments, most of the progress has come from systematic testing and development. In this section we will discuss the configurations, operating frequencies, and pumping speeds of several sources and compare their performance.

To illustrate some of the practical aspects of ECR sources we will first compare three different "mature" ECR sources, MINIMAFIOS,[28] ECREVIS, [29] and the LBL ECR.[30-32] Then we will discuss the recently developed MINIMAFIOS-16GHz ECR source. Each source represents a different design philosophy and different design features. MINIMAFIOS is designed to be compact, economical, and easy to operate. ECREVIS is a large superconducting source patterned after SUPERMAFIOS. The LBL ECR is similar in size to MINIMAFIOS but designed for maximum pumping speed in the second stage. In spite of the design differences, each source has been used successfully for cyclotron and atomic physics applications.

The design of MINIMAFIOS is illustrated in Fig. 3. This source evolved from MICROMAFIOS and has been developed for reliable operation and uncritical tuning. It has a single RF feed for both stages located in the axial field maximum between first and second stage. Feeding in the RF power at this point reduces RF transmission problems which can take place in a plasma between the location of the upper hybrid mode and the ECR zone. Both stages have magnetic mirror configurations. The axial magnetic field is produced by water cooled copper coils which use ~ 100 kW. The radial magnetic field is produced by a $SmCo_5$ hexapole.

B_z

L (cm)

ECR2   ECR2   ECR1

0,5 T
0,36 T

75   50   25   0

UHF

S5   S4   S3   S2   S1
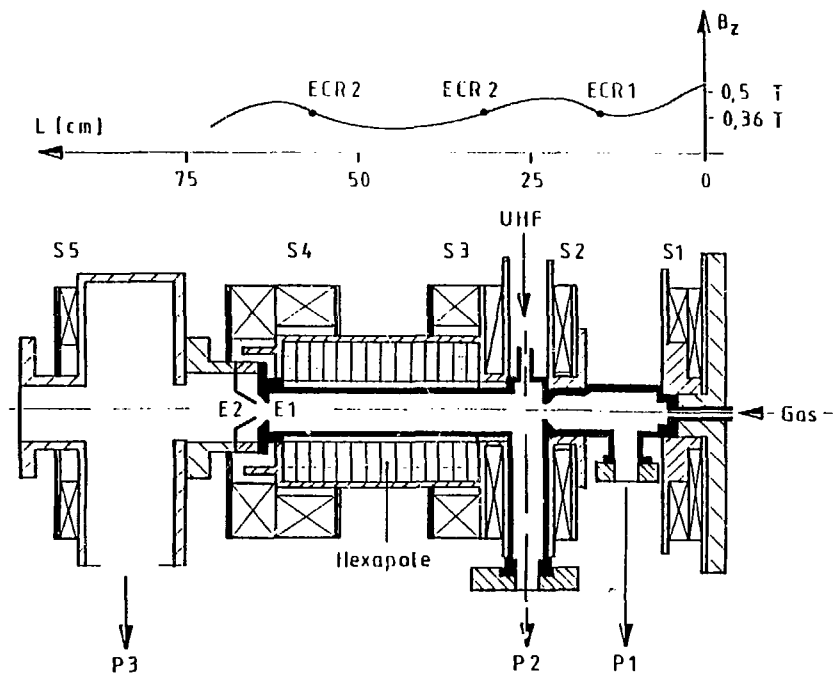
E2 E1

Gas

Hexapole

P3   P2   P1

Fig. 3 Schematic drawing of MINIMAFIOS and the axial magnetic field distribution. S1 through S5 are solenoid coils. ECR1, ECR2, and ECR3 indicate the location of the ECR resonances on axis. A single RF feed for the first and second stages is located between coils S2 and S3.   XBL 8611-4405

6.

Turbo-pumps provide pumping for each stage of the source.

Figure 4 illustrates the large superconducting ECR source, ECREVIS, which was patterned after SUPERMAFIOS. This source provided beam for the Louvain-la-Neuve cyclotron for 3 years before it was replaced by a smaller room temperature source, OCTOPUS. ECREVIS had separate klystrons and separate RF feeds for the first and second stages. The first stage operated on the downhill gradient of the magnetic field at an RF frequency of 14 GHz. The second stage RF frequency was 8.5 GHz and the typical operating power was 3 kW. Both the second stage solenoid field and hexapole field were supplied by superconducting coils. The cryostat was very efficient using only .25 l/hr of liquid helium and had a 500 l helium capacity. This meant that it could operate for more that 2 months on a single liquid helium transfer. The pumping for each stage is provided by second generation diffusion pumps.

Figure 5 illustrates the basic design features of the LBL ECR. Two distinguishing features of the LBL ECR are the relatively low second stage frequency and high pumping speed in the plasma chamber. The first stage uses a 1 kW 9.2 GHz klystron (typical power 100 W) and the second stage uses a 3 kW 6.4 GHz klystron (typical power 400 W). The first stage operates on the uphill gradient of the axial magnetic field as shown in Fig. 6. The radial magnetic field is produced by a $SmCo_5$ sextupole with radial slots which allow radial pumping. The axial magnetic field is produced by tape wound edge cooled copper coils, each powered by an individual supply for maximum flexibility in magnetic field configuration. Typical magnet power is 30 kW.

The performance of these three sources for neon and argon is illustrated in Fig. 7 and Fig. 8, respectively. These curves represent published values for the analyzed currents from these sources.[28,29,34] They represent a summary of measurements on the sources with various tunings to optimize individual charge states and therefore are not actual charge state distributions. The measured intensities depend on the acceptance of the analyzing system and the emittance and intensity of the ECR sources. The three analyzing systems are similar, so the measured intensities should be a reasonable gauge of source performance. Figure 7 shows that for intermediate neon charge states MINIMAFIOS produces higher intensities and for high charge state neon the LBL ECR produces slightly higher intensities. The neon intensities for ECREVIS are remarkably similar considering ECREVIS is about 4 times as large in all dimensions as the other two sources. Figure 8 shows MINIMAFIOS produces higher intensities of intermediate charge state argon, while ECREVIS and the LBL ECR produce more very high charge states. This may reflect the relatively low pressure, low plasma density mode in which ECREVIS and the LBL ECR operate. Jongen suggested that ECREVIS operated best at a low pressure ($\sim 5 \times 10^{-7}$ Torr) in the second stage because the large plasma volume resulted in a relatively low plasma density. To produce the best Ar^{14+} currents with the LBL ECR requires operating at low second stage pressures ($\sim 3 \times 10^{-7}$ Torr) and in a mode with reduced total extracted current. It also requires mixing a high percentage of oxygen with a very small percentage of argon. Good first stage performance seems critical for the production of the very high charge state ions and having independent control of the first stage parameters makes it
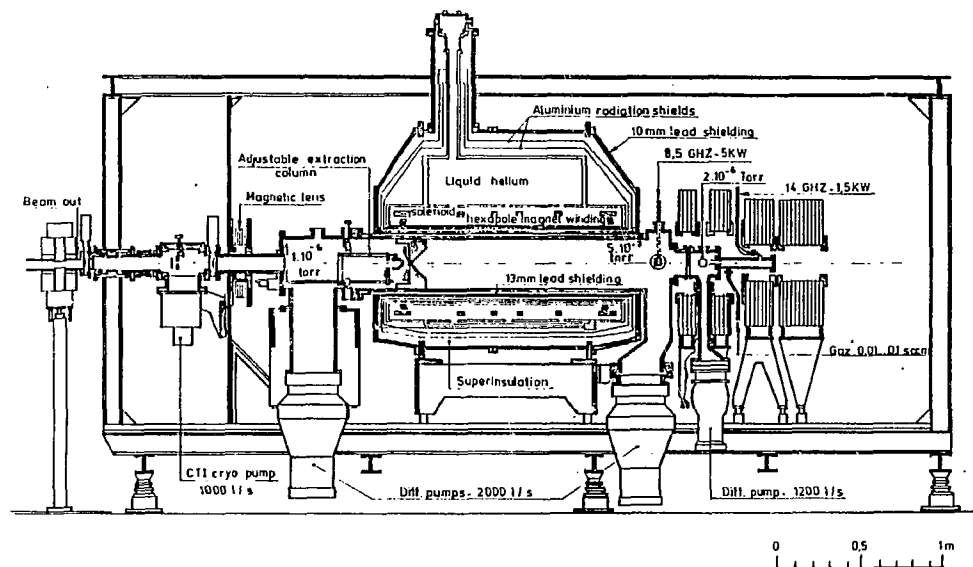
Fig. 4 Design of the large superconducting source ECREVIS in its final configuration. The lead shielding around the plasma chamber and outside the cryostat was used to attenuate a large x-ray flux generated by the source.   XBL 8611-4406
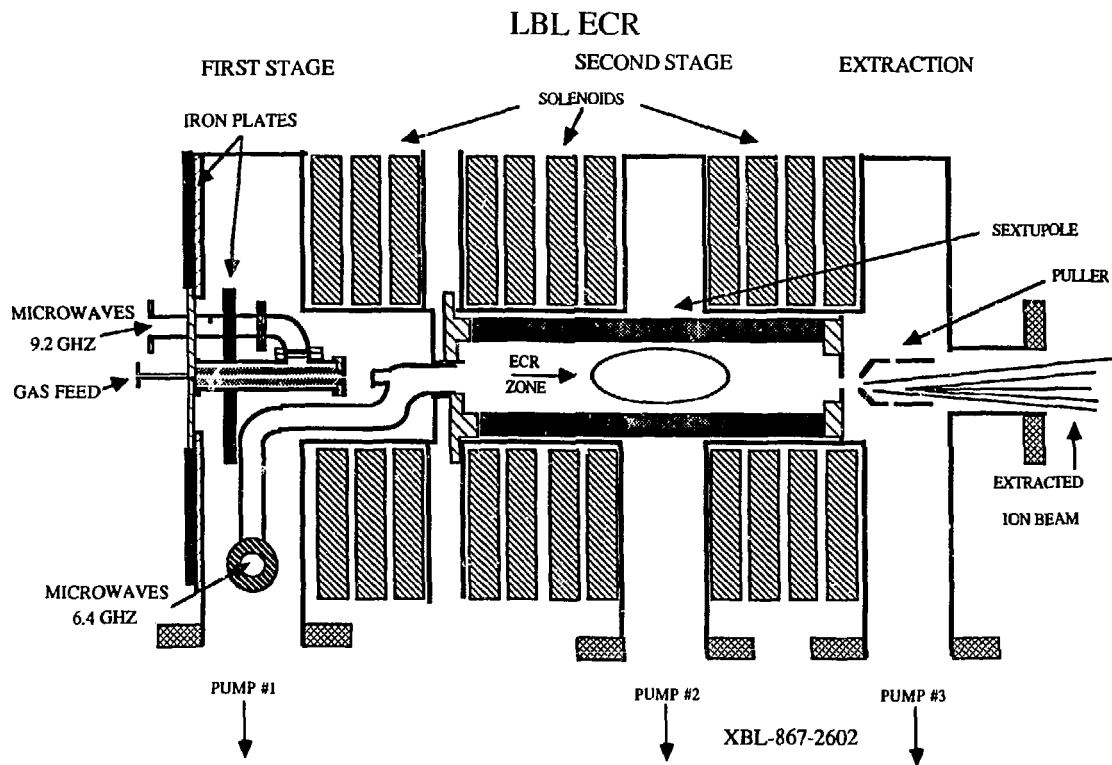
11.

LBL ECR

Fig. 5 Schematic drawing showing the main features of the LBL ECR source. A new first stage and two iron plates to increase the magnetic field in the first stage were added during 1985.
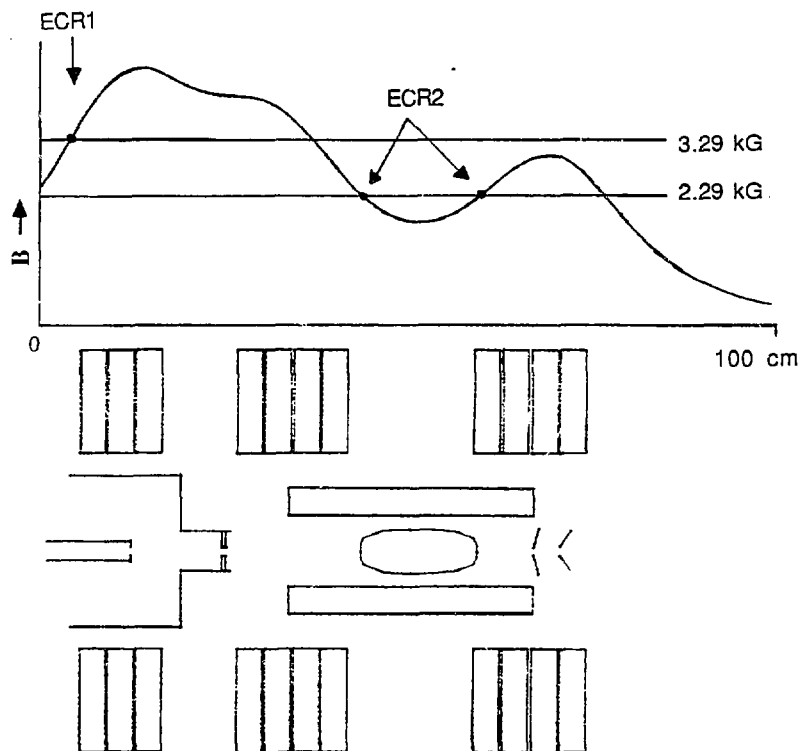
Fig. 6 Axial magnetic field distribution and schematic view of the LBL ECR showing the location of the solenoid coils, sextupole, extraction, and ECR zone. ECR1 is the location of the ECR zone in the first stage, ECR2 shows the locations of the zone on axis in the second stage.

XBL 8611-4407

Fig. 7 Comparison of extracted Ne currents from MINIMAFIOS, ECREVIS, and the LBL ECR. The curves represent a summary of measurements on the sources with various tunings to optimize individual charge states.   XBL 8611-4408
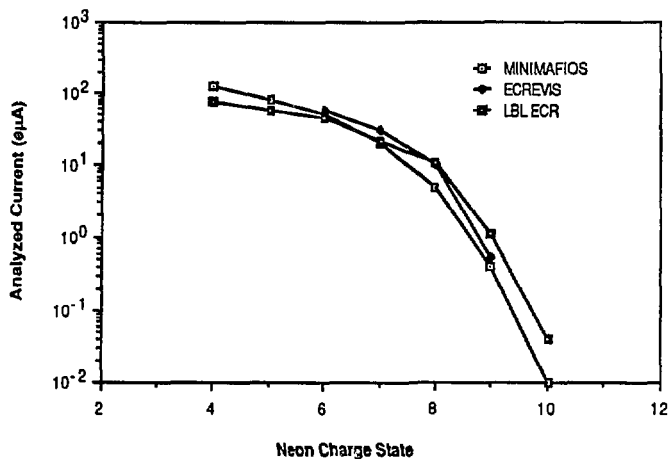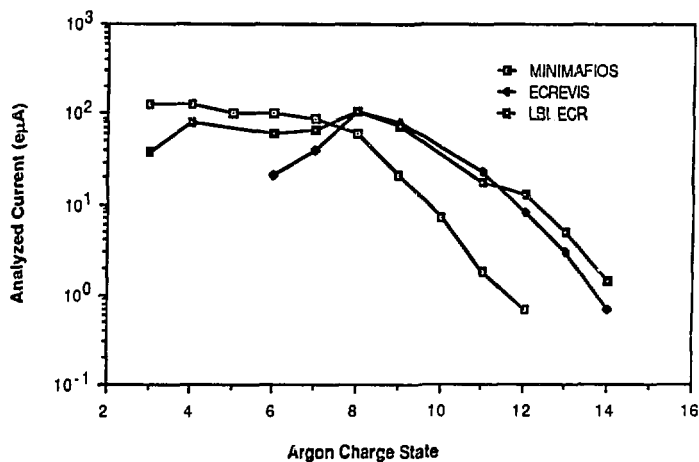

Fig. 8 Comparison of extracted Ar currents from MINIMAFIOS, ECREVIS, and the LBL ECR. The curves represent a summary of measurements on the sources with various tunings to optimize individual charge states.   XBL 8611-4409

easier to optimize the first stage output.

Recently, Geller et al[33] have developed an upgraded version of MINIMAFIOS called MINIMAFIOS-16GHz. This source illustrated in Fig. 9 differs from the classical MINIMAFIOS in four main respects. First, it operates at 16.6 GHz rather than 10 GHz. Second, it has no pumping in the first or second stage, relying solely on plasma pumping. Third it has a new $SmCo_5$ hexapole which produces .8T at the poles. Fourth, it is operated in a pulsed mode with a pulse length of 150 ms and a repetition rate of 1 Hz. One goal of this project was to show that by increasing the RF frequency from 10 to 16.6 GHz it is possible to increase the n_e by $\sim(1.66)^2$ and thereby increase $n_e\tau_i$. Therefore the source was designed to operate at either 10 or 16.6 GHz. Even though its hexapole was optimized for the higher frequency mode, its operation at 10 GHz was quite similar to the classical MINIMAFIOS. At 16 GHz they found that the total extracted current increased 3 fold as predicted, that the currents for intermediate charge state neon increased 3 fold and the current for fully stripped neon increased ~200 fold to 1 eµA. The large increase in the fully stripped neon current indicates an increase in $n_e\tau_i$. The analyzed currents for neon from MINIMAFIOS-16GHz are compared to those for the classical MINIMAFIOS and the LBL ECR in Fig. 10. After the 15 kW 16.6 GHz klystrons failed, the source was modified to operate with an 18 GHz klystron and is now called MINIMAFIOS-18GHz. One of these sources is being developed for installation on the injector linac for the SPS at CERN and will be used to produce ~40 eµA of S^{12+} in the spring of 1987.

Operation of the LBL ECR with the 88 Inch Cyclotron.

The LBL ECR source, injection beam line and cyclotron center region have performed reliably since coming into regular operation in January 1985. Since then about 80% of the cyclotron operating schedule has been with the ECR source. The light-ion filament source is used only for runs of two or more shifts in length using proton, ^{3}He, or alpha beams. Occasionally the polarized ion source is used. The heavy-ion PIG sources are no longer used. The operating experience with the Cyclotron+ECR has been highly successful in terms or reliability, stability, production of high charge state currents, and in the range of ions which can be produced. The improved operation of the accelerator has resulted in a significant increased demand for beam time. Many new beams have been developed which has enabled the physicists to do experiments previously impossible at the 88-Inch Cyclotron. For example: a 32.5 MeV/u $^{16}O^{8+}$ was used in a nuclear structure experiment, a $^{36}Ar^{18+}$ with a total energy of 1.08 GeV was used to test the response of scintillator materials to intermediate energy heavy ions, and a ^{48}Ca beams between 200 and 400 MeV were used used in fission cross section measurements with gold and lead targets.

The performance of the LBL ECR is summarized in Tables 2 and 3. All results are given for an extraction voltage of 10 KV and 12 mm analyzer slit widths except for xenon where 6 mm slits were used to improve the resolution . The currents represent the best results taken from many tests. Larger currents can be obtained at higher extraction voltage. For example,
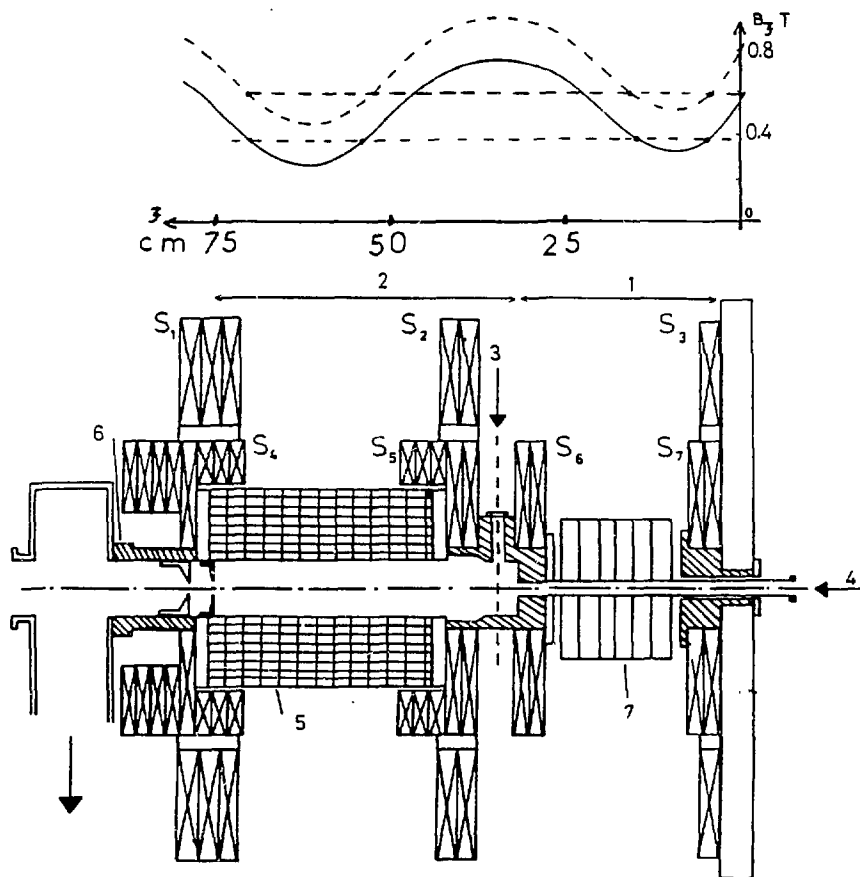
Fig. 9 Schematic drawing of the new MINIMAFIOS-16GHz ECR source and the axial magnetic field distribution. S1 through S7 are solenoids, 1 is the first stage, 2 the second stage, 3 the RF feed, 4 gas injection, 5 hexapole, 6 extraction, and 7 heat radiator. The only pump used is in the extration region.[31]   XBL 8611-4410
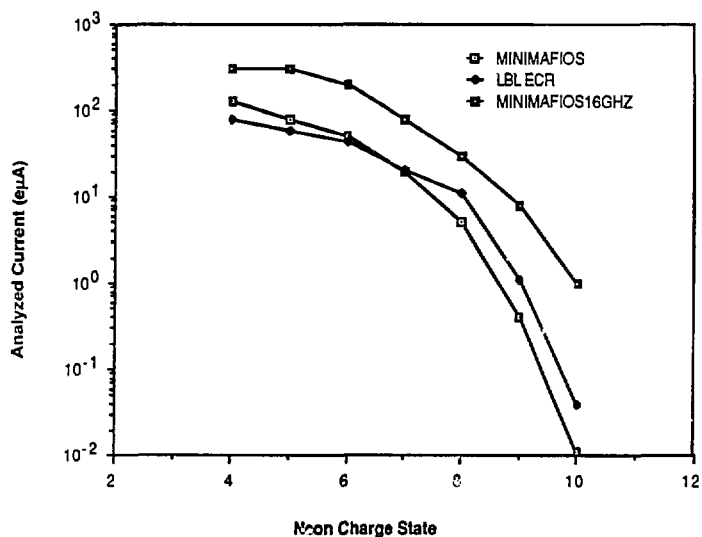
Fig. 10 Comparison of extracted Ne currents from the new MINIMAFIOS-16GHz, MINIMAFIOS, and the LBL ECR. The curves represent a summary of measurements on the sources with various tunings to optimize individual charge states. The largest fractional improvement with the 16 GHz source occurs for fully stripped neon. XBL 8611-4411

TABLE 2
Currents for the LBL ECR: Hydrogen through Silicon

CS	^{1}H	^{3}He	^{12}C	^{14}N	^{16}O	^{19}F	^{20}Ne	^{24}Mg	^{28}Si
1+	300	300	27	82	118				
2+		200	37	117	143	43	51	32	20
3+			*	106	152	55	63	34	33
4+			31	110	*	53	78	28	69
5+			6.5	93	96	37	58	44	72
6+				19	82	17	45	34	47
7+					14	11	21	18	30
8+					0.95	1	11	8	17
9+						0.05	1.1	6.3	7
10+							0.04	2.2	2.7
11+								0.1	0.5
12+									0.2

TABLE 3
Currents for the LBL ECR: Sulfur through Xenon

CS	^{32}S	^{39}K	^{40}Ar	^{40}Ca	^{48}Ti	^{84}Kr	^{127}I	^{129}Xe
3+	10	4	38	23				
4+	*	4.5	82	24				
5+	20	5	*	*				
6+	*	8.5	60	37		9		
7+	63	11	66	38	2.4	12		
8+	*	18	106	36	*	22		
9+	36	37	72	31	12	25		4.1
10+	*	22	*	*	10	22	4.2	4.7
11+	5	12	18	22	8	19	4.9	5.1
12+	*	2.4	13	11	*	*	5.7	5.2
13+	.4		5	3.2	1	21	7.5	5.2
14+	*		1.4	1.1		*	8.5	5
15+	.001		*	*		16	11	4.3
16+			0.03	0.03		8	*	4.6
17+						7	12	4.3
18+						*	15	4.4
19+						2	15	4.8
20+						0.9	14	4.8
21+						*	*	4
22+						0.1	11	3.5
23+							10	3.1
24+							8.3	2.7
25+							5.6	2
26+							2.1	1.1
27+							0.83	0.34
28+							0.2	
29+							0.05	
30+							0.009	

All currents in eµA measured at 10 kV extraction voltage.
* Indicates not measured because a mixture of two ions with identical charge to mass ratios were present.
Natural isotopic abundance source feeds were used except for ^{3}He and ^{22}Ne^{10+}

the current for Ar^{8+} increased from 106 µA at 10 kV to 140 µA at 14 kV. This is due in part to a decrease in the transverse emittance at high voltage. The ^{84}Kr and ^{129}Xe currents were produced using natural krypton and xenon, respectively, so higher currents could be obtained with mono-isotopic gases. To a large extent the ion beam development has been dictated by the needs of the cyclotron users. For elements such as nitrogen, oxygen, and argon that have been frequently used the values in the tables are well optimized. Other beams such as fluorine, sulfur, and titanium have been infrequently used and the performance will probably improve with further development.

Several different techniques have been used to produce beams from the LBL ECR and these techniques are summarized in Table 4. Elements which exist in gaseous form are most easily used in the ECR source. A flexible gas manifold system which allows up to three gases to be used simultaneously has been installed on the LBL ECR. The gases can be injected into either the first or second stage of the source. The best proton and alpha beams are produced by feeding the gas directly into the second stage and turning off the first stage. For all elements heavier than oxygen, gas mixing is used to enhance the high charge state performance of the source. Although it remains a point of discussion why, all ECR sources seem to benefit from gas mixing. In all cases adding a light mixing gas enhances the high charge states of the heavier gas. The presence of heavy ions in the plasma also acts to depress the charge state performance of light ions. For example, a very small percentage of xenon in the plasma decreases O^{7+} currents by as much a factor of 10. Prior to the installation of a new first stage, which is described in more detail elsewhere,[34] the high charge states of oxygen and nitrogen could be enhanced by the addition of helium. After the installation of the new first stage, the high charge state performance for oxygen and nitrogen was considerably better and mixing helium no longer helped. In general oxygen works better as a mixing gas in the LBL ECR than nitrogen. One possible reason is that the first stage performance is better with oxygen than nitrogen. A CSD for oxygen measured on the LBL ECR is shown in Fig. 11. For this measurement the source was tuned to maximize O^{7+}. The main impurities in the CSD are hydrogen, carbon, and nitrogen.

Beams from elements such as carbon, sulfur and silicon can be produced using gaseous compounds such as CH_4, SO_2, and SiH_4, respectively. In general to take advantage of gas mixing effects, compounds with lighter atoms bonded to the desired element are chosen. For the LBL ECR geometry injecting the compound gases into the second stage and the mixing gas into the first stage produces the most consistent results. The pressure in the first stage cavity is relatively high ($\sim$3 x10^{-4} Torr) and using compounds in it may result in plating the walls which can affect first stage performance. Also, since operation with the cyclotron frequently requires several different beams in a week and only a few hours is allowed for beam changes, contamination of the first stage would cause operational problems. An additional advantage to injecting the gaseous compounds into the second stage comes from the reduced gas flows required. Typically the first stage requires about 15 std cc/hr of gas, while the second stage requires at least an order of magnitude lower flow. Particularly when corrosive gases are used,

TABLE 4

Techniques Used to Produce Beams from the LBL ECR

Beam	Starting Material	Stage/Oven*	Temp ^oC	Mixing gas (stage)[#]
Protons	H_2 gas	2		none
Alphas	He gas	2		none
Carbon	CO_2 or CH_4 gas	2		oxygen (1)
Nitrogen	N_2 gas	1		none
Oxygen	O_2 gas	1		none
Fluorine	CHF_3 gas	2		oxygen
Neon	Ne gas	1		oxygen or helium (1)
Magnesium	Mg metal	Oven	400	oxygen or nitrogen (1)
Aluminum	Al_2O_3 rod	Into plasma		oxygen(1)
Silicon	SiH_4 gas	2		oxygen (1)
Sulfur	SO_2 gas	2		oxygen (1)
Potassium	KCl & Ca	Oven	450	oxygen (1)
Argon	Ar gas	1		oxygen (1)
Calcium	Ca metal	Oven	480-570	oxygen or nitrogen (1)
Titanium	TiF_4 powder	Oven	100	oxygen
Krypton	Kr gas	1		oxygen (1)
Niobium	Solid rod	Into plasma		oxygen(1)
Iodine	I crystals	Oven	25	oxygen (1)
Xenon	Xe gas	1		oxygen (1)
Bismuth	Bi metal	Oven	525	oxygen (1)

* Indicates whether the primary gas was injected into the first or second stage or if the oven was used.

[#] Indicates if a mixing gas was used and if so into which stage it was injected.
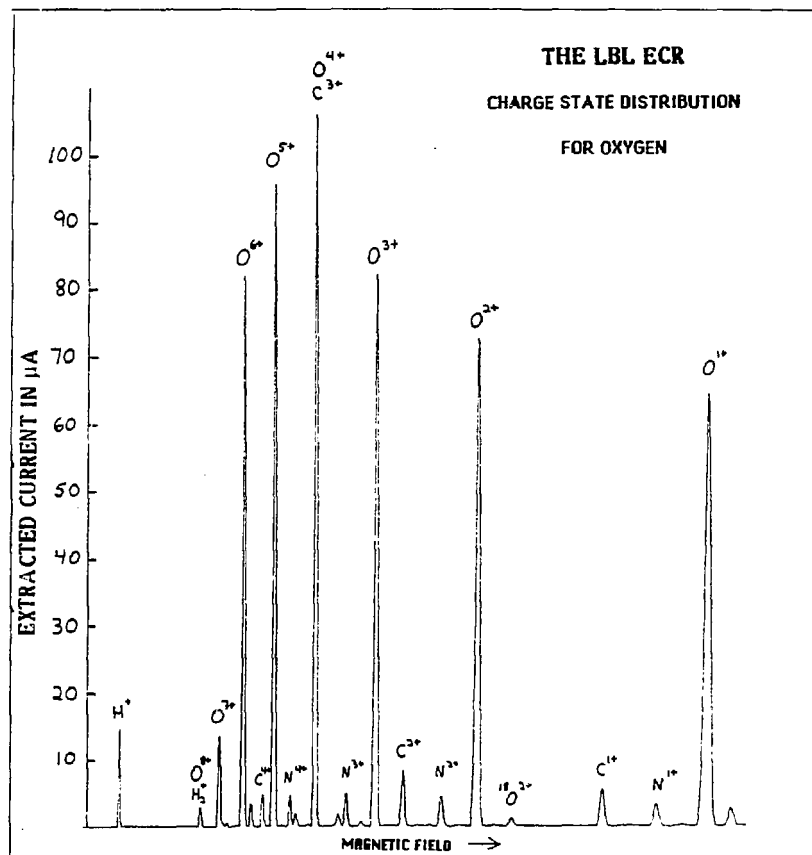
Fig. 11 Charge state distribution for oxygen measured on the LBL ECR. The plot was
produced on an x-y recorder by slowly sweeping the analyzing magnet.   XBL 8611-4412

it is a significant advantage for pump lifetime to minimize the gas throughput. Other advantages of injecting compounds into the second stage are easier source tuning and better long term stability. To avoid handling problems associated with fluorine gas, Freon 23 (CHF_3) is injected into the second stage.

A variety of metallic ion beams can now be produced from the LBL ECR using a simple resistance heated oven as shown in Fig. 12. The oven is inserted radially into the second stage so that vaporized metal atoms stream through the ECR plasma and are ionized by electron impact. Typically with oven operation, the plasma is maintained by running either oxygen or nitrogen as a support gas in the first stage. This is similar to the use of a mixing gas when operating the source with gases heavier than oxygen. The amount of metal in the plasma is adjusted by varying the oven temperature. A proportional temperature controller is used to keep the oven temperature constant. The beam stability with the oven is quite remarkable. A number of cyclotron runs lasting several days have used the metal ion beams from the ECR source. During some of these runs no adjustment of the ECR source or oven was required. This is quite important from the point of view of operations, since the cyclotron is run by a single operator per shift and no one is available to make frequent source adjustments during the night.

For calcium the measured usage was found to be in good agreement with the mass flow rate calculated using the conductance of the oven nozzle and the vapor pressure of calcium at the operating temperature. Typical operating conditions to produce 10 μA Ca^{11+} beam from the ECR are an oven temperature of 507 °C which corresponds to a calcium vapor pressure of 1×10^{-3} Torr and a calcium usage rate of 2.1 mg/h. Similar results were obtained with magnesium using oven temperatures corresponding to Mg vapor pressure of 1 to 3 $\times 10^{-3}$ Torr.

For many nuclear physics experiments only very low intensity beams are necessary. An experiment to study the cross sections for fission using $^{48}Ca^{11+}$ beams from 200 to 400 MeV on ^{197}Au and ^{208}Pb was recently completed at the 88-Inch Cyclotron. The oven was operated at 476 °C and was loaded with a piece of enriched calcium (54% ^{48}Ca). In 68 hours of operation only 10 mg of the enriched calcium were consumed, which corresponds to 0.15 mg/h. During the run the $^{48}Ca^{11+}$ beam from the ECR was .6 μA and the beam extracted from the cyclotron was typically 25 nA depending somewhat on energy and cyclotron tuning.

In Fig 13 the CSD for iodine and bismuth are plotted. Both bismuth and iodine are mono-isotopic which makes the measurement of the CSD easier than using multi-isotope elements such as xenon. ^{209}Bi was chosen to explore the performance of the LBL ECR source for very heavy elements because it is mono-isotopic and its vapor pressure temperature characteristics are appropriate for the oven. The best results were produced with an oven temperature of 526 °C. As shown in Fig 13 the source produced .56 eμA of Bi^{31+} and .055 eμA of Bi^{34+}. These charge states would be quite useful for the high K superconducting cyclotrons at MSU, Milan, and Texas A&MU as well as the upgraded heavy-ion linac at ANL.

A slightly different technique was used to produce potassium beams from the ECR source[35] The oven was loaded with a mixture of KCl and Ca and heated to 450 °C. Inside the oven chamber the calcium reacts with the KCl forming $CaCl_2$ and potassium vapor. This
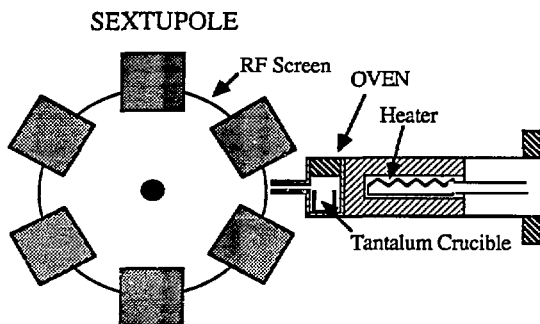
LBL ECR

SEXTUPOLE

Fig. 12. A cross section view showing the radial position of the oven with respect to the sextupole structure. The source material is loaded into the tantalum crucible, which inhibits liquid film flow. The oven temperature is monitored and controlled using a type K thermocouple and a commercial proportional temperature controller.   XBL 867-2604
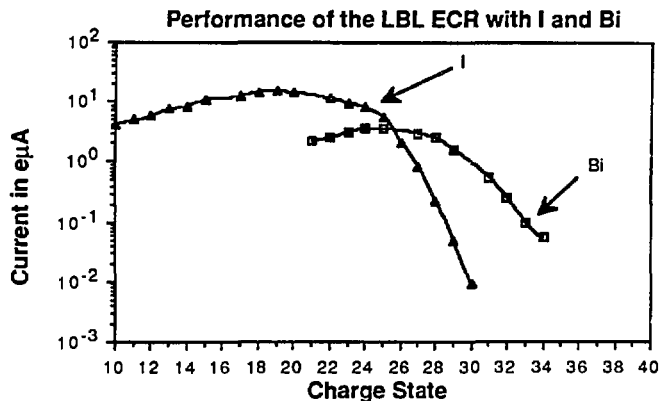

Fig 13 Performance of the LBL ECR with ^{127}I and ^{209}Bi. The best iodine beams were produced from iodine adsorbed on the walls after the oven was removed. The bismuth beams were produced by running the oven at 526 °C.   XBL 8611-4413

technique avoided the problems associated with handling potassium metal, reduced the chlorine beam, and made a very stable, easily controlled potassium ion beam in the ECR. The ratio of potassium to chlorine in the plasma was about 40 to 1. This method should work equally well with all of the alkali metals. A stable titanium beam was produced using TiF_4 in the oven at 100°C to produce a molecular vapor of TiF_4 which dissociates in the plasma. The maximum intensity of the titanium is limited by increase in neutral pressure caused by the accompanying fluorine atoms. However, this technique circumvented the problems of building an oven capable of 1500 °C, as would be required to produce a sufficient vapor pressure of titanium from the metal.

Another technique used to produce beams from solids is to insert a rod into the edge of the plasma.[28] This technique has been used in the LBL ECR to produce Al, Fe, Ti, and Nb beams, which have been used for test purposes and atomic physics measurements but not for operation with the cyclotron. The solid rods are inserted radially into the second stage plasma until they are heated to sufficient temperature by the hot electrons in the plasma to produce the required metal vapor pressure. The heating rate is a function of plasma density, axial magnetic field strength and RF power. With careful tuning it is possible to produce stable beams for several hour periods. In order to use this method for operating with the cyclotron, a feedback control system operating either the rod's position or RF power level needs to be developed.

Operation of the LBL ECR with solids for the cyclotron involves some compromises. Usually after solids are used there is a short term degradation in the high charge state performance of the source. The degree of degradation and the length of the recovery time depends on the type and amount of material injected into the source. Two mechanisms appear to cause the degradation. First, if a high mass solid has been run it can provide a background of heavy ions in the plasma via recirculation with the walls. These heavy ions then act as negative gas mixing, depressing the lighter ion CSD. Second, contamination of the walls reduces the plasma stability making it impossible to operate the source with the parameters used when it is clean. The most effective method for cleaning the source after a metallic ion run seems to be to run it with oxygen in a mode producing a large total current. To minimize operating problem with metals, we keep the metal vapor density in the plasma as low as possible consistent with producing sufficient beam intensity for the experiment. Also, when possible we schedule a non-critical run such as O^{5+} or light ions after the metal ion run to give the source time to recover.

The horizontal and vertical sections of the beam transport system from the ECR source to the center of the cyclotron are shown in Fig 14 and Fig 15. Magnetic rather than electrostatic elements were chosen because of better space charge neutralization for high intensity beams, fewer vacuum penetrations, and better long term reliability. Magnetic steering coils are used at each lens. Beam diagnostics consist mainly of fixed four jaw collimators with beams readouts before each set of lenses where the beam is largest. A movable 4 jaw collimator and Faraday cup are provided near the top of the vertical line. Beam at the bottom of the vertical line can be read on the mirror electrode in the midplane of the cyclotron and then on the cyclotron beam
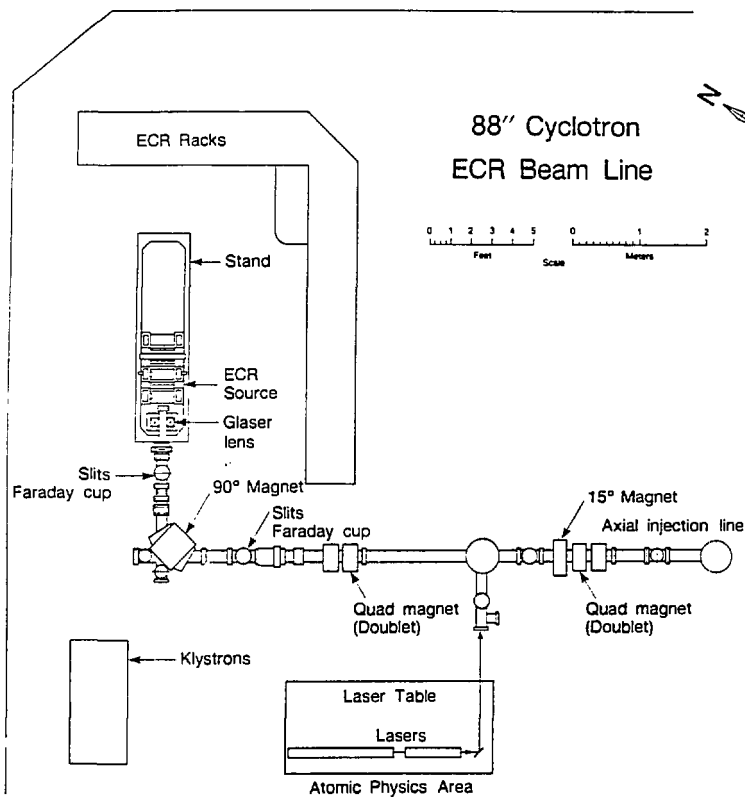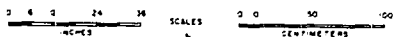
88″ Cyclotron
ECR Beam Line

Fig. 14 Plan view of the LBL ECR source and horizontal injection line located on the vault roof above the 88-Inch Cyclotron. The beam can be deflected out of the horizontal line to the atomic physics area by a 90° electrostatic deflector.
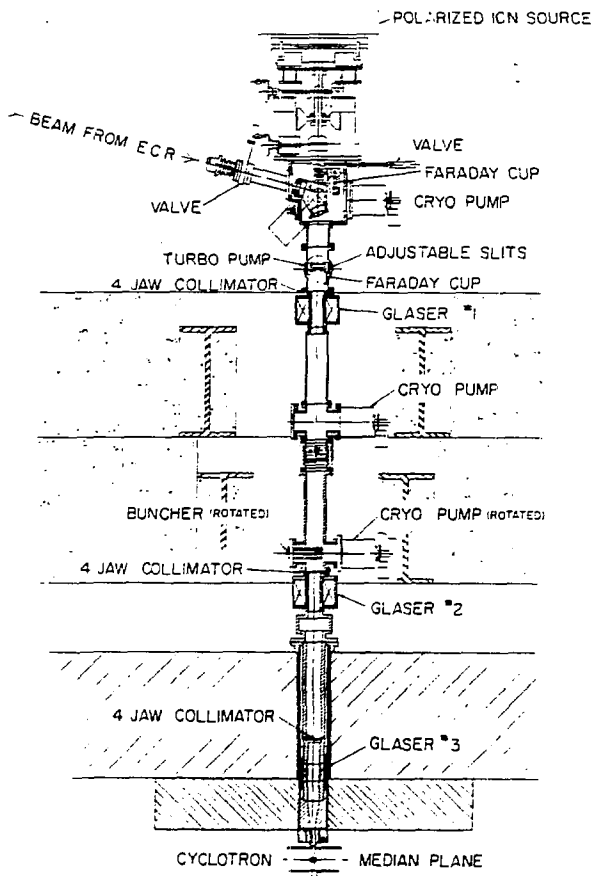
Fig. 15 Schematic view of the axial injection line of the 88-Inch Cyclotron. The ECR beam is first bent 15 degrees in the vertical plane by a magnet in the horizontal line and then by 75 degrees by a magnet at the top of the axial line. This was necessary because of the location of the polarized ion source.

probe at small radius. The vacuum system uses cryo-pumps and turbo-pumps and all metal seals. The typical beam line pressure is $< 5 \times 10^{-8}$ Torr which is sufficiently low so that beam loss due to charge exchange with neutrals is negligible. To minimize beam steering due to the stray field of the cyclotron, nickel plated magnetic steel beam pipes were used where possible and magnetic shielding was added to stainless steel components such as bellows. A simple gridded two gap sine wave buncher installed slightly above the cyclotron yoke provides a factor of 3 to 5 transmission gain over an unbunched beam. A gridded mirror is used to bend the beam through 90 degrees into the midplane.

The calculated beam profiles from the exit of the ECR source to the cyclotron midplane are shown in Fig. 16. The currents of the focussing and bending elements are now predicted by a small computer program based on a combination of calculations and beam line tuning experience. The predictions are sufficiently accurate that the operator only needs to do some fine tuning to maximize the beam. In Table 5 some examples of beams from the cyclotron+ECR are listed. The transmission from the Faraday cup after the analyzing magnet to extracted beam from the cyclotron varies from a few percent up to 17% depending on the cyclotron main field, harmonic number used, and vacuum in the cyclotron tank. Usually the source is operated at 10 kV which gives good beam centering for the maximum dee voltage of 50 kV.

Future of ECR Sources

The successful coupling of ECR sources to cyclotrons, a synchrotron, and soon to a heavy-ion linac[36] make it clear that continued development of ECR source technology is essential. This is a relatively young technology and further improvements are to be expected. These improvements may come in an incremental way as a result of refinements in extraction geometry, first stage performance, source vacuum, or other area. They may come in a more dramatic fashion, if higher frequencies RF sources such as gyrotrons can be successfully used to drive ECR sources. Since the power density must rise with the plasma density, as the source frequency increases the size should decrease. Comparison of the performances of small and large sources give no clear indication that $n_e \tau_i$ scales with source size, although there may be a relationship between RF wavelength and minimum plasma chamber size.[30] This is consistent with higher frequencies and smaller sources. A key issue is finding a way to increase the the plasma density without increasing the neutral density. This is particularly important for producing very high charge states for ions in the mass range from 50 to 238. Additional areas for improvement include application of plasma diagnostics to ECR sources and a better theoretical understanding of high charge state production in ECR sources. Better techniques need to be developed for producing beams from solids. Ovens such as the one used with the LBL ECR can probably not be used above 1000 $^{\circ}$C. One possibility would be to build an electron beam heated oven which operates in the edge of the axial magnetic field. Another possibility would be to use a laser to evaporate high temperature materials at the edge of the plasma.

There are many challenges and room for new ideas in the field of ECR sources. We can look forward to real advances in the field as new groups join in the development of ECR sources.

References

1. H. Postma, Phys. Lett.31A,196,(1970)

2. S.Bliman, R. Geller, W. Hess, B. Jacquot, C. Jacquot, IEEE Trans. NS-19, No 2., 200,(1972)

3. A. van der Woude, IEEE Trans. NS-19, No. 2, 187(1972)

4. R. Geller, IEEE Trans. NS-23,No. 2,904,(1976)

5. Yu.V. Gott, . M.S. Ioffe, and Telkosky, Nuclear Fusion, Suppl. Part 3 (1962) 1045

6. R. Geller, IEEE Trans. NS-26, No. 2, 2120,(1979)

7. H. Tamagawa, I. Alexeff, C.M. Jones, and P.D. Miller, IEEE Trans. NS-23, No. 2, 994 (1976)

8. Y Jongen, C. Pirart, G. Ryckewaert,and J. Steyart, IEEE Trans. NS-26, No 2,2160(1979)

9. V. Bechtold, N. Chan-tung, S. Dousson, R. Geller, B. Jacquot, and Y. Jongen, N.I.M. 178,305(1980)

(10) V. Bechtold, L. Friedrich, and H. Schweickert, Proceedings of the 9th Int'l Conf on Cyclotrons and Their Applications, 249 (1981)

11. G. Fuchs, IEEE Trans. NS-19,160,(1972)

12. N. Teraura, H. Tamagawa, ISIAT 3,21,Kyoto(1979)

13. S. Bliman, N. Chan-Tung. J. Plasma Phys. 8,(1979)

14. Y. Jongen, int. rep. ref. LC8001 Laboratoire du Cyclotron, Univ. Cath. De Louvain, Belgium (1980)

15. H. West, int. rep. ref. UCRL-53391 Lawrence Livermore Nat. Lab., (1982)

16. J. Hesse and K. Wiesemann, ISIAT, Tokyo(1984)

17. D. H. Crandal, Pyssica Scripta. 23,pp 153-162(1981)

18. W. Lotz, Zeitschrift für Physik 216, 241(1968)

19. A. Müller, Phys. Lett. 113a, 415(1986)

20. A. Muller, E. Salzborn, R. Frodl, R. Becker, H. Klein, and H. Winter, J. Phys B: Atom. Molec.Phys13,1877(1980)

21. Private communication, E. Salzborn.

22. Y. Jongen, Proceedings of the 10th Int'l Conf on Cyclotrons and their Applications, pp. 322-327, E. Lansing, MI, (1984)

23. K Bernhardi and K. Wiesemann, Plasma Physics 24(8),pp 867,884(1982)

24. D.L. Smatlak, X. Chen, R.C. Garner, D.L. Goodman, S.A. Hokin, J.H. Irby, B.G. Lane, D.K. Liu, R.S. Post, D.K. Smith, and J. Trulsen, "Experimental Results From The Constance B Magnetic Mirror," Internal Report MIT Plasma Fusion Center, PFC/RR-86-15(1986)

25. Private communication, Y. Jongen

26. F.W. Meyer, "Operation of the ORNL ECR Source" Proceedings of the 7th ECR Ion Source Workshop, Jülich, H. Beuscher Editor,(1986)

27. H. Kohler and K. Weisemann, "Energy Distribution of Ions Extracted from a 5 GHz ECR Source," Proceedings of the 7th ECR Ion Source Workshop, Jülich, H. Beuscher Editor(1986)

28. R. Geller, B. Jacquot, and M. Pontonnier, Rev. Sci. Instr. 56,1505(1985)

29. J.L. Bol, Y. Jongen, M. Lacroix, F. Mathy, and G. Ryckewaert, IEEE Trans. NS-32,1817(1985)

30. C.M. Lyneis and D.J. Clark, IEEE Trans. NS-32,no 5, 1745 (1985)

31. C. Lyneis, Nucl. Instr. and Meth. in Phys. Res. B 10/11, 775 (1985)

32. D.J. Clark, Y. Jongen, and C.M. Lyneis, Proceedings of the 10th Int'l Conf on Cyclotrons and their Applications, pp. 133-136,E. Lansing, MI, (1984)

33. R. Geller, B. Jacquot, and P. Sortais, Nucl. Inst. and Meth. A243, 244(1986)

34. C.M. Lyneis, "Recent Developments of the LBL ECR Ion Source, Proceedings of the 7th ECR Ion Source Workshop, Jülich, H. Beuscher Editor,(1986)

35. Private communication, M. Prior

36. R. Pardo, E. Minehara, F Lynch, P. Billquist, W. Evans, B.E. Clifft, and M. Waterson, "Status of the ATLAS PIIECR Ion Source Project," Proceedings of the 7th ECR Ion Source Workshop, Jülich, H. Beuscher Editor,(1986)
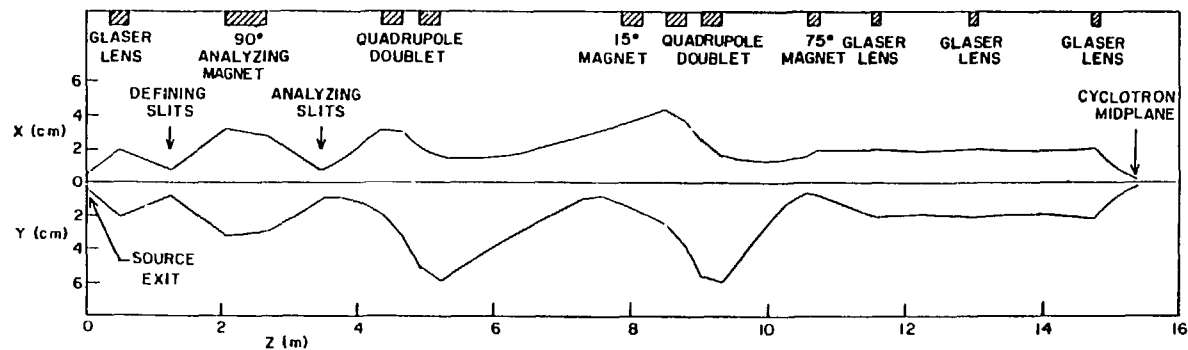
XBL 845-1775

Fig. 16 Calculated beam profiles in the horizontal and vertical planes from the exit of the ECR source to the 88-Inch Cyclotron midplane. For the calculation the emitance was assumed to be 200π mm-mrad, unnormalized.

TABLE 5

Optimized beams from the 88-Inch Cyclotron+ECR

Ion	Cyclotron Energy (MeV)	Harmonic	Source Current (eμA)	Cyclotron Ext. Current (eμA)	Transmission (%)
$^{14}N^{5+}$	180	1	60	7	11
$^{18}O^{5+}$	117	1	60	10	17
$^{16}O^{6+}$	315	1	40	3	7
$^{16}O^{7+}$	429	1	10	0.2	2
$^{22}Ne^{6+}$	151	1	40	7	17
$^{24}Mg^{7+}$	192	1	20	1.5	7
$^{28}Si^{6+}$	180	1	60	3	5
$^{40}Ar^{12+}$	504	1	6	.2	3
$^{16}O^{2+}$	20	3	69	2	3
$^{40}Ar^{9+}$	180	3	30	3	10
$^{86}Kr^{14+}$	301	3	2.5	.08	3
$^{129}Xe^{21+}$	451	3	.8	.02	3
$^{16}O^{2+}$	20	5	67	.15	0.2